Unprecedented Behavior of (9 R)-9-Hydroxystearic Acid-Loaded Keratin Nanoparticles on Cancer Cell Cycle

Unprecedented behavior of (*9R*)-9-hydroxystearic acid loaded keratin nanoparticles on cancer cell cycle

Alberto Busi,‡ Annalisa Aluigi,¶ Andrea Guerrini,¶ Carla Boga,‡ Giorgio Sartor,† Natalia Calonghi,† Giovanna Sotgiu,¶ Tamara Posati,¶ Franco Corticelli,# Jessica Fiori,§ Greta Varchi¶*and Claudia Ferroni¶*

‡Department of Industrial Chemistry, University of Bologna, Viale Risorgimento 4, 40136 Bologna, Italy

¶Institute for the Organic Synthesis and Photoreactivity, National Research Council, Via Gobetti 101 - 40129 Bologna, Italy

†Department of Pharmacy and Biotechnology, University of Bologna, Via Irnerio 48, 40126 Bologna, Italy

#Institute for Microelectronics and Microsystems, National Research Council, Via Gobetti 101, 40129 - Bologna, Italy

§Department of Chemistry "G. Ciamician", University of Bologna, Via Selmi 2, 40126, Bologna, Italy

KEYWORDS (*9R*)-9-hydroxystearic acid, keratin, nanoparticles, drug-induced aggregation, histone deacetylases, cell cycle, cell membrane.

ABSTRACT Histone deacetylases, HDACs, have been demonstrated to play a critical role in epigenetic signaling and were found to be overexpressed in several type of cancers, therefore they represent valuable targets for anticancer therapy. 9-Hydroxystearic acid has been shown to bind the catalytic site of HDAC1, inducing G0/G1 phase cell cycle arrest and activation of $p21^{WAF1}$ gene, thus promoting cells growth inhibition and differentiation in many cancer cells. Despite the (*R*) enantiomer of 9-hydroxystearic acid (9R) displayed promising *in vitro* growth-inhibitory effect on HT29 cell line, its scarce water solubility and micromolar activity require novel solutions for improving its efficacy and bioavailability. In this work, we describe the synthesis and *in vitro* biological profiling of 9R keratin nanoparticles (9R@ker) obtained through an in-water drug-induced aggregation process. The anticancer activity of 9R@ker was investigated in HT29 cell line: the results indicate an increased fluidity of cell membrane and a higher intracellular ROS formation, resulting in an unexpected S phase cell cycle arrest (25% increase as compared to the control) induced by 9R@ker as respect to free 9R and an induction of cell death.

INTRODUCTION

Human cancer progression is the result of both genetic alteration and epigenetic changes. In particular, the deregulation of lysine residues acetylation in histones 3 and 4 seems to play a pivotal role not only in cancer development,[1] but also in tumor invasion and metastasis.[2] Histone deacetylation catalyzed by histone deacetylases (HDACs) silences gene transcription by promoting chromatin condensation.[3–5] The expression of individual HDACs has been shown to be altered in several tumors. In particular, HDAC1 was overexpressed in breast, ovarian, gastric, prostate and colon carcinomas,[5] thus representing a potential attractive target for anticancer therapy.[6,7] Besides, the increased activity of HDAC could result in a transcriptional repression of tumor-suppressor genes, such as $p21^{WAF1}$ gene, a cell cycle cyclin-dependent kinase inhibitor whose expression is down-regulated in different kinds of cancers.

Recently, several natural and synthetic compounds have been identified as HDAC inhibitors (HDACi), which exert a significant anticancer effect by promoting differentiation, cell-cycle arrest and apoptosis. Despite the relatively weak activity of aliphatic acids as HDACi, long-chain mono-hydroxyl fatty acids have gained increasing interest due to their biological effect on DNA synthesis and cell proliferation. Among these, 9-hydroxystearic acid (9-HSA), an endogenous lipid, whose content is strongly diminished in cancer cells, demonstrated to inhibit HDAC1 activity at micromolar concentrations,[9] leading to the histone hyperacetylation with consequent inhibition of cancer cells growth and differentiation.[10–15] In HT29 human colorectal adenocarcinoma cells, the inhibitory effect of 9-HSA is mediated by an arrest in G0/G1 phase cell cycle and by a direct activation of $p21^{WAF1}$ gene.[16]

Molecular docking studies had shown a favorable formation energy of the HDAC1−9-HSA complex; in particular, by separately administering both enantiomers, the complex with (*9R*)-9-HSA (abbreviated hereafter as 9R) resulted to be more stable with respect to that formed with 9*S*.[6,17,18]

Despite a clinical advantage, the use of 9R shows some limitations such as the extremely poor water solubility and the need of administering relatively high compound doses in order to have a pharmacological effect. In this regard, drug delivery systems could overcome pharmacokinetic and pharmacodynamic drawbacks, improve water solubility and allow diminishing the drug dose due to enhanced tumor-site accumulation *via* active and passive mechanisms.[19] To this end, hydroxyapatite nanocrystals were recently prepared with growing concentrations of 9R (up to 8.6 wt %) and tested for the potential local treatment of bone metastasis.[18] The composite nanocrystals, when administered to SaOS-2 osteosarcoma cells, showed cytostatic and cytotoxic effects modulated by hydroxystearate content.[20] Despite these promising results, their application as antiproliferative agents is mainly restricted to bone tumor cells. Among the plethora of biomaterials for drug delivery, protein-based nanoparticles (NPs) represent a valuable alternative approach. In fact, proteins display key features which are of the utmost importance for biomedical/pharmaceutical applications: they are non-toxic, biodegradable, low immunogenic, easy to functionalize with drugs and targeting ligands, and in many

cases naturally abundant;[21,22] Moreover, proteins contain hydrophobic and hydrophilic domains that can be exploited for accommodating both hydrophilic and hydrophobic drugs, such as 9R. In the last years, keratin has emerged as a very promising biomaterial in the drug delivery field; in particular, our group has recently described the synthesis of keratin-based nanoparticles through different preparation procedures (desolvation, self-assembling, gelation and drug-induced aggregation).[23–27] Keratin is the most abundant non-food, structural protein that can be recovered from several waste sources, such as byproducts of the textile industry and meat slaughtering.[28] Furthermore, it possesses excellent biocompatibility and low toxicity to cells, which make it particularly attractive for drug delivery purposes.

Based on these considerations, we focused our study on the synthesis of 9R loaded keratin nanoparticles (9R@ker) obtained through the spontaneous aggregation of hydrosoluble and high molecular weight keratin induced by 9R in water. The 9R@ker antiproliferative effect was preliminarily evaluated in three different human colon cancer cell lines further investigated in HT29 cell line, and compared with free 9R and 9R albumin loaded NPs (9R@HSAr), being albumin the reference biomaterial in the field of drug delivery mediated by protein nanoparticles.[29]

EXPERIMENTAL SECTION

Materials. Keratin was kindly supplied by Kerline Srl (Bologna – Italy). 9R was synthesized and characterized as previously reported.[18] Recombinant human serum albumin, fluorescein isothiocyanate isomer I and all other chemicals used for the NPs formulation were purchased from Sigma-Aldrich (Italy). *Dimorphoteca sinuata L.* seeds were purchased from Galassi Sementi (Gambettola, FC, Italy). Deuterated 9-HSA (*d*9) was prepared as previously described.[6]

Synthesis of 9R loaded keratin nanoparticles (9R@ker). Keratin powder (9 mg) was dissolved in H_2O mQ (18 mL) at room temperature and the solution was sonicated for 30 minutes and filtered (0.45 μm) in order to remove possible aggregates. 0.2 mL of 9R in ethanol (2.5 mg/mL) was slowly added to the keratin solution under stirring (700 rpm). As determined by dynamic light scattering

(DLS) analysis, twenty minutes after 9R addition 9R@ker were formed and freeze-dried. 9R@ker stability in physiological conditions was determined by dissolving 500 μg of keratin NPs, in 2 mL of PBS and stored at 37°C. NPs dimensions were then periodically controlled by DLS measurements using a NanoBrook Omni Particle Size Analyzer (Brookhaven Instruments Corporation, USA) equipped with a 35mWred diode laser (nominal 640 nm wavelength).[27]

9R loading and release from nanoparticles. In order to determine the drug release profile of 9R from keratin NPs, 1mL of 9R@ker dispersion (7 mg/mL), was placed into a dialysis bag (cut-off 12-14 kDa), and immersed under shaking in 17 mL of a PBS solution at pH 7.4, or in 17 mL of a PBS solution at pH 5.5 at 37°C.[27] Periodically, the outer solution was withdrawn, while further 17 mL of PBS were added back to the incubation media.[28] 9R was extracted from buffer with dichloromethane and the combined organic layers were concentrated. The sample and a known amount of an internal standard, 2,4-dinitrotoluene (2,4-DNT), selected because its NMR signals do not overlap with those of 9R, were mixed together, dissolved in 0. 7 mL of $CDCl_3$, and transferred to a 5-mm NMR tube. A quantitative value of the sample can be calculated using the following eqn (1):

$$m_x = \frac{A_x}{A_{std}} \times \frac{N_{std}}{N_x} \times \frac{MW_x}{MW_{std}} \times \frac{P_{std}}{P_x} \times m_{std} \qquad (1)$$

where *A* are integrated areas under the peaks, *N* is the number of protons in the considered functional group, *m* are the prepared masses, *MW* the molecular weights and *P* the purities, *x* indicates 9R, while *std* the internal standard.

The drug release was evaluated by quantitative proton NMR spectrometer operating at 500 MHz at 25°C (Agilent NMR DD2 500 MHz equipped with single ADC console and OneNMR™ probe). The qNMR experiments were performed following the optimized protocol described by Yang et al.[30-32] The peak at δ 2.37 ppm (2H, t), corresponding to the methylenecarboxy group of 9R, was selected as the analytical signal for quantitative purposes. The ^{1}H-NMR spectrum of 2,4-DNT exhibited the characteristic signals of three aromatic protons at δ 8.84 (d, J = 2.5 Hz, 1H), 8.37 (J = 2.5 Hz, J = 8.55 Hz, 1H), 7.58 (d, J = 8.6 Hz, 1H), and of methyl protons at δ 2.74 ppm (3H, s, CH_3). In particular, the signals at δ 8.37 ppm have been utilized for the quantification (Figure S2).[30] The 9R release

profiles were analyzed by curve-fitting analysis with different mathematical models, using ORIGIN 8.1 ® software (OriginLab Corporation, MA, USA).[26]

Nanoparticles characterization. The hydrodynamic diameter of the nanoparticles in aqueous solution (0.5 mg/mL) was determined by DLS at 25°C, using a NanoBrook Omni Particle Size Analyser (Brookhaven Instruments Corporation, USA) equipped with a 35 mW red diode laser (nominal 640 nm wavelength). As for the electrophoretic mobility, ζ-potential was measured at 25°C by means of the same system. Scanning electron microscopy (SEM) images were obtained by using a Zeiss EVO LS 10 LaB6 microscope, with an acceleration voltage of 5 kV, and a working distance of 5 mm. Samples for SEM analysis were prepared by drying a drop of nanoparticle solution (0.5 mg/mL) in the SEM specimen mount at room temperature, followed by gold spattering.[23] The thermogravimetric analysis (TGA) measurements were carried out using a TA Instruments STD Q600 (10 °C/min, room temperature to 600 °C, air flow).

The FTIR spectra were acquired by using the attenuated total reflectance technique (ATR) with a Bruker Vertex 70 interferometer equipped with a diamond crystal using a reflection Platinum ATR accessory, in the 4000 – 600 cm^{-1} range, with 100 scans and a resolution of 4 cm^{-1}. In order to study the protein secondary structure, the spectra in the 1580-1750 cm^{-1} region were corrected and smoothed with an eleven-point Savitsky-Golay function. Resolution of the amide I band was performed by means of Gaussian shape related to different protein secondary structures. The results of the fitting procedure were further evaluated by investigating the residual from the difference between the fitted and the original curve when the R^2 value was higher than 0.99.[33]

Circular Dichroism spectra were measured using a Jasco model J-720 CD spectrometer (Japan Spectroscopic Co., Tokyo, Japan). Sample aqueous solutions spectra (50 μg/mL) were acquired in the 205-240 nm range at 25°C and with a one cm^{-1} path length.

Cell culture and treatments. The human colon carcinoma cell lines HT29 and HCT116 as well as the normal embryonic intestinal cell line I407 were obtained from the American Type Culture

Collection (Rockville, MD, USA). Caco-2 cell line was kindly provided by Dr. Marianna Barbalinardo (National Research Council - Institute of Nanostructured Materials, ISMN).

All cell lines were grown in RPMI 1640 medium (Labtek Eurobio, Milan, Italy), supplemented with 10 % FBS (Euroclone, Milan, Italy) 2 mM L-glutamine (Sigma-Aldrich, Milan, Italy) at 37°C, and 5% CO_2. Cells were seeded at 1.5 x 10^4 cells/well onto 6-well plates (Orange Scientific, Braine-l'Alleud, Belgium). After 24 h, all cell lines were incubated with 50 μM 9R or 9R@ker for 24, 48 and 72 h, respectively and untreated cells were used as a control. Moreover, HT29 were seeded onto 6-well plates and after 24 h were treated with 9R, or 9R@ker, or 9R@HSAr, or @ker, or keratin at the concentration of 50 μM, or 12R@ker, or 12R at the concentration of 10 μM. Trypan Blue exclusion dye method was used to determine the number of viable cells.

Cell uptake studies. HT29 were seeded in 6-well plastic dishes containing 10 mm cover slips for 24 h. @FITC:ker and 9R@FITC:ker solutions (50 μM) were added to the cell culture media and after 15 or 60 minutes of incubation at 37°C, cells were washed three times with PBS. The cover slips were put on slides and analysed using a Nikon C1s confocal laser-scanning microscope, equipped with a Nikon Plan Apo 60X, 1.4-NA oil immersion lens.

Nile Red Staining. Stock solutions of Nile Red (NR, 9-diethylamino-5H-benzo[alpha]phenoxazine-5-one, Sigma-Aldrich, Milan, Italy) 1 mM in DMSO were prepared and stored protected from light. Cells were seeded at 2x10^4 cells/cm^2 on glass cover slips and treated with 9R@ker, or 9R@HSAr, or 12R@ker for 1 h respectively, and then incubated with 5 μM NR for 5 min at 37 °C. After treatments, cells were washed twice with PBS, fixed with 3% paraformaldehyde, and washed again with 0.1 M glycine in PBS. Subsequently, the samples were washed with 1% BSA in PBS, embedded in Mowiol and analysed using a Nikon C1s confocal laser-scanning microscope, equipped with a Nikon Plan Apo 60 X, 1.4-NA oil immersion lens.[34]

In situ detection of ROS generation. The intracellular oxygen free radicals' generation after 9R@ker treatment was investigated through fluorimetric assay using the probe dichlorodihydrofluorescein diacetate (DCFH-DA), (ThermoFisher Scientific, Waltham, MA). HT29

cells were exposed to 100 μM tert- butylhydroperoxide (TBH), (Sigma-Aldrich, Milan, Italy) as a positive control for the DCFH-DA assay. Cells were washed twice in PBS and incubated with 5 μM DCFH-DA for 15 min at 37°C. DCF fluorescence was measured by using an EnSpire Multimode Plate Reader (PerkinElmer, Waltham, MA) at the excitation and the emission wavelengths of 485 nm and 535 nm, respectively.

Fluorescence anisotropy measurements. The plasma membrane fluidity of HT29 cells was evaluated by measuring the fluorescence anisotropy of the hydrophobic probe 1-4-Trimethylammoniumphenyl-6-Phenyl-1,3,5-Hexatriene (TMA-DPH) (ThermoFisher Scientific, Waltham, MA). HT29 cells were treated with 9R@ker or 12R@ker, then washed three times with PBS and suspended at a final concentration of 3×10^5 cells/mL. The cell suspension absorbance was maintained less than 0.15 at the excitation wavelength of TMA-DPH. A few microliters of TMA-DPH stock solution were added to the cell suspension with the aim of obtaining a final probe concentration of 1μM. Fluorescence anisotropy measurements were performed by using a PTI QuantaMaster fluorimeter (Photon Technology International, North Edison, NJ) equipped with a temperature-controlled cell holder and Polaroid HNP'B polarizers. Temperature was kept at 25°C. Excitation and emission wavelengths were set at 360 nm and 430 nm, respectively.

Cell-Cycle Analysis by Flow Cytometry. HT29 cells were seeded in 25 cm^2 flasks at a density of 2 x 10^4 cells/cm^2. The effects on the cell cycle were studied 24 h after treatment with 50 μM 9R, or 9R@ker, or 9R@HSAr, or @ker, or keratin, or 10 μM 12R@ker, or 12R. Cells were detached with 0.11% trypsin, washed in PBS, and centrifuged. The pellet was suspended in 0.01% Nonidet P-40, 10 μg/mL RNase, 0.1% sodium citrate, 50 μg/mL PI, for 30 min at room temperature in the dark. PI fluorescence was analyzed using a Beckman Coulter Epics XL-MCL flow cytometer, and cell analysis was performed using the M cycle (Verity) and MODFIT 5.0 software.[34]

Total protein extraction and Western Blot. HT29 cells were seeded in 25 cm^2 flasks at a density of 2 x 10^4 cells/cm^2 and after 24 h treated with 50 μM of 9R or 9R@ker. Twenty-four hours after, both treated and control cells were washed twice with PBS and lysed for 20 min in a buffer containing

(40 mmol/l HEPES, pH 7.4, 60 mmol/l glycerophosphate, 20 mmol/l p-nitrophenyl phosphate, 0.5 mmol/l Na_3PO_4, 250 mmol/l NaCl, 1% Triton X-100, 0.5 mmol/l PMSF, and 10 mg/ml each of aprotinin, leupeptin, pepstatin and antipain, (Sigma-Aldrich, Italy) at 0°C. Cell lysates were then centrifuged at 12000 x g for 20 min, supernatants were collected and protein concentration was determined by using the Bio-Rad protein assay method (Bio-Rad, Hercules, CA). The proteins were resolved on a 10% density gel and immunoblotted with p21 or Bax or β-actin mouse antibodies 1:1000 (Cell Signaling Technology, Danvers, MA). Detection of immunoreactive bands was performed with a secondary antibody conjugated with horseradish peroxidase diluted 1:20000 (Amersham, Uppsala, SE) and developed with the enhanced chemiluminescence system Clarity Western (Bio-Rad, Hercules, CA) and quantification was done by Fluor-S Max MultiImager (Bio-Rad) using β-actin signal as control.[35]

Histone extraction and Western Blot. HT29 cells were seeded in 25 cm^2 flasks at a density of 2 x 10^4 cells/cm^2, cultured with 50 μM 9R, or 9R@ker, or 9R@HSAr, or @ker, or keratin, or with 10 μM 12R@ker, or 12R for 6 h, and the histone portion was directly extracted. Cells were collected using 0.11% trypsin and 0.02% EDTA, washed twice with PBS, and nuclei were isolated as previously reported.[36] Histones were extracted and western blot analysis was performed using a 10% polyacrylammide gel electrophoresis, as previously described.[6] The nitrocellulose membrane was incubated with primary antibody specific for acetylated lysine, and then with secondary Horseradish Peroxidase-conjugated antibody (GE Healthcare, Chicago, IL). After several washes with PBS-TWEEN 20 0.1%, antibody binding was detected as described in the previous section.

Quantitative Real Time-PCR analysis. HT29 cells were seeded in 25 cm^2 flasks at a density of 2 x 10^4 cells/cm^2 and treated with 9R or 9R@ker for 6 hours. Total RNA was isolated by RNeasy Tissue kit (Qiagen, Hilden, Germany) according to the manufacturer's protocol.[34] Briefly, 1 μg of RNA was reverse-transcribed with Transcription High Fidelity cDNA Synthesis kit (Roche Diagnostics, Manheim, Germany) by using random hexamer primers. Quantitative Real Time PCR (qRT-PCR) analyzed the cDNA, by employing the Light Cycler Fast Start DNA Master SYBR Green I Kit and

the Light Cycler 2.0 instrument (Roche Diagnostics, Manheim, Germany). Gene expression was quantified by $\Delta\Delta C_T$ method, by using *G3PDH* as the housekeeping gene. The following primers were used: 5'-ATTTGGTCGTATTGGGCGCC-3' (forward) and 5'-ACGGTGCCATGGAATTTGCC-3' (reverse) for *G3PDH* detection, 5'-GATGCGTCCACCAAGAAGC-3' (forward) and 5' – CCGCCACAAAGATGGTCAC-3' (reverse) for *BAX* detection; 5'-CCTAAGAGTGCTGGGCATTTT-3' (forward) and 5'- TGAATTTCATAACCGCCTGTG-3' (reverse) for *p21* detection.[34]

Statistical analysis. All experiments were repeated at least three times, on three independent samples. Data are presented as mean ± SD and Student's T test was used for repeated measurement values. A *p* value below 0.05 was considered significant.

RESULTS AND DISCUSSION

9R@ker synthesis and characterization

Keratin powder was dissolved in mQ water and 9R@ker NPs were obtained through a drug-mediated aggregation process, which allows for the quantitative formation of stable NPs, whose dimension and polydispersity index depend on 9R loading (Figure 1A). An initial optimization study allowed to determine the optimal 9R concentration (in ethanol) to be used for particles formation, which resulted to be 2.5 mg/mL. Under these conditions, e.g. [ker] 1 mg/mL and [9R] 2.5 mg/mL, particles' hydrodynamic diameter ranges from 162 to 308 nm for 9R loading going from 10 to 36% of protein weight, respectively (Figure 1A). Figure 1A shows that the polydispersity index is partially correlated to the 9R loading, thus increasing when increasing 9R loading.

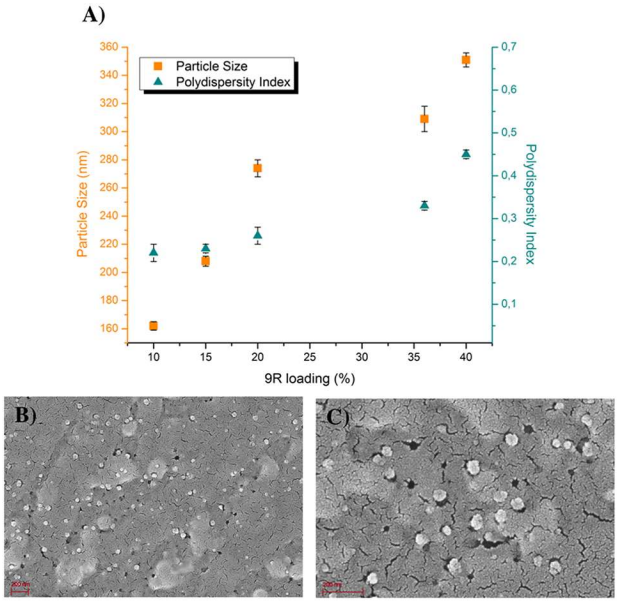

Figure 1. A) Correlation between 9R loading and keratin nanoparticles dimension (orange squares) or polydispersity index (green triangles) and data of keratin nanoparticles obtained by drug-induced aggregation method. B and C) SEM images of 9R@ker NPs deposited on atomic flat silicon.

These preliminary studies allowed to establish the optimal parameters for nanoparticles preparation: a drug loading of 10% wt/ker_{wt} allows to obtain stable and highly reproducible NPs with an average diameter of 162 ± 2 (PDI < 0.2 ± 0.2), and a ζ-potential of -43 ± 1 mV. It is worth noticing that this methodology in combination with keratin allows to reach a 9R loading ratio higher with respect to those obtained with hydroxyapatite, e.g. 10% *vs* 8.6%.[18] Furthermore, since the preparation of stable 9R@ker does not require either chemical stabilization or purification processes, e.g. centrifugation, ultrafiltration and dialysis, we can assume that both nanoparticles yield and drug loading are quantitative. As indicated by the ζ-potential value, 9R@ker in water have a negative surface charge, probably due to the presence of the SO_3^- and COO^- groups on the keratin backbone. NPs morphology was further analyzed by SEM, which confirmed the particles spherical shape and an average dry diameter of 72 nm (Figure 1B and 1C).[23] The difference in the NPs radii measured with DLS and SEM could be attributed to the diverse environment in which analysis were carried out, e.g. water or air, respectively.[37,38]

The keratin folding induced by 9R was studied by FTIR spectroscopy and Circular Dichroism (CD). Figure 2A reports the FTIR spectra of keratin powder and 9R@ker; both spectra are characterized by the adsorption peaks of peptide bonds such as the amide A (3800-3120 cm^{-1}), related to the N-H stretching vibrations, the amide I (1700-1600 cm^{-1}) originating mainly from the C=O stretching vibration, the amide II (1580-1480 cm^{-1}), due to the N-H bending and C-H stretching vibrations and the amide III (1300-1200 cm^{-1}) due to the in-phase combination of C-N stretching and N-H in plane bending vibration.[39] Moreover, peaks centered at 1025 and 1190 cm^{-1} derive from the symmetric and asymmetric S=O stretching vibrations of the cystein-S-sulphated groups of keratin (Bunte salts), respectively.[26,40] Instead, the triplet peak between 3000 and 2800 cm^{-1} derives from the C-H stretching vibrations of CH_2 and CH_3 group. This peak is more intense in the nanoparticles because of the aliphatic chains of 9R.

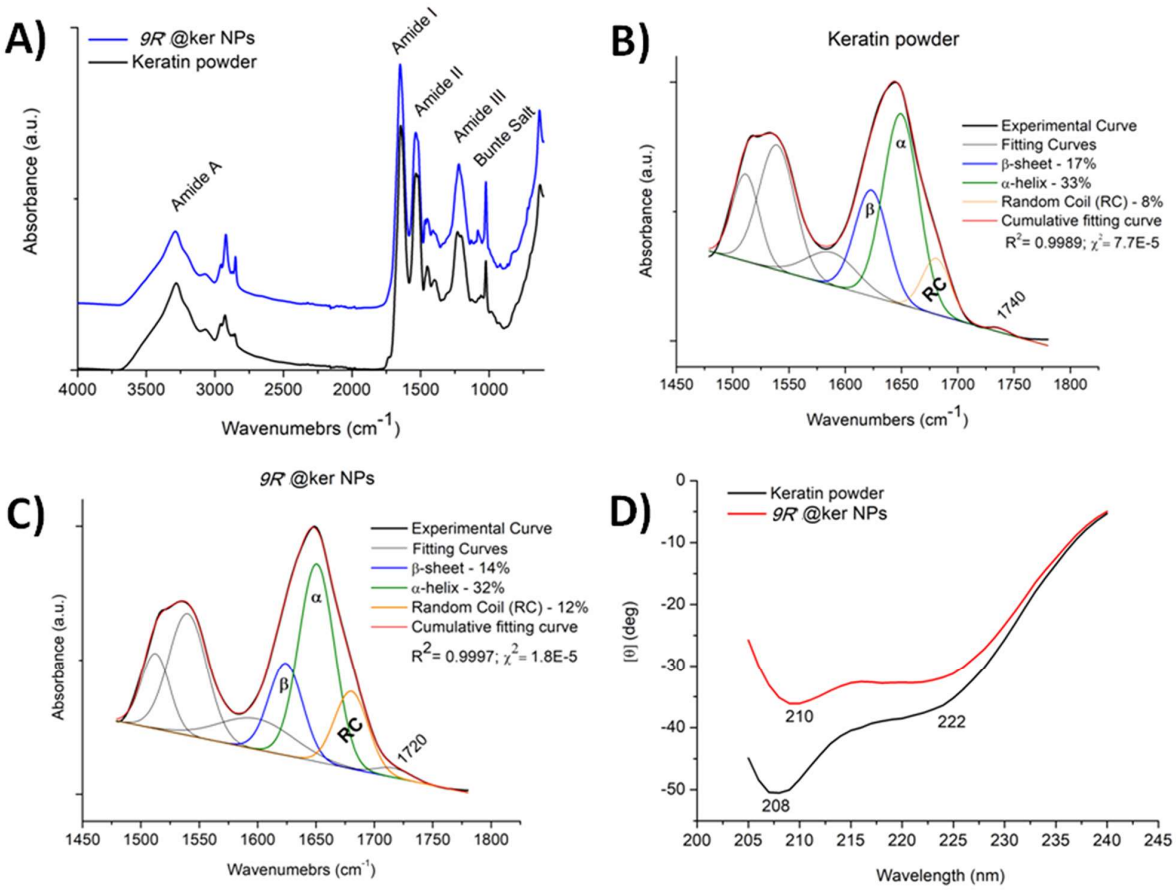

Figure 2. FT-IR and Circular Dichroism studies. A) FTIR spectra of keratin powder and 9R@ker NPs; B) Amide I curve fitting of keratin powder; C) Amide I curve fitting of 9R@ker NPs and D) circular dichroism spectra of keratin powder and 9R@ker NPs.

Since Amide I band is highly sensitive to small variations in the protein's molecular geometry, it can be exploited for the analysis of protein secondary structures. Therefore, Gaussian bands were used to resolve the Amide I and Amide II spectral regions (1480-1780 cm^{-1}) of keratin powder and 9R@ker (Figures 2B and 2C). In order to estimate the protein secondary structure ratio, the area under the peaks associated to a specific folding was integrated and normalized for the Amide I and Amide II total area.[26] Figure 2B and 2C showed that 9R@ker was characterized by a slightly decrease of the β-sheet keratin structures accompanied by a slight increase of the unordered/random coil structures. Moreover, the adsorption peak at 1740 cm^{-1} of the keratin powder and relative to the COO^- stretching vibrations, is shifted to lower wavenumbers in the nanoparticles (1720 cm^{-1}), suggesting that the interactions between the protein and 9R involve end-chains carboxylic groups.

In addition, keratin powder shows two negative bands at 208 nm and 222 nm, that is the typical CD pattern of proteins rich in α-helix structures (Figure 2D).[41] On the other hand, in the 9R@ker the peak at 208 nm has a lower ellipticity and a broadening towards 210 nm, confirming the increase of the disordered structures of the protein.[42]

Nanoparticles stability and *in vitro* 9R release

NPs stability studies were carried out in PBS at 37°C by monitoring particles diameter during time by DLS measurements. As shown in Figure 3A, a slight increase from 170 nm to 236 nm occurs within the first 24 hours, while no significant changes were observed in the polydispersity index. These data suggest a good stability of 9R@ker under physiological conditions.

The release profile of 9R from NPs was determined through a quantitative proton NMR experiment. 9R@ker were placed into dialysis bags, immersed in PBS at i) pH = 7.4 (physiological conditions), and at ii) pH = 5.5 in order to mimic the typical lysosomes acidic conditions (Figure 3C).[31,43,44]

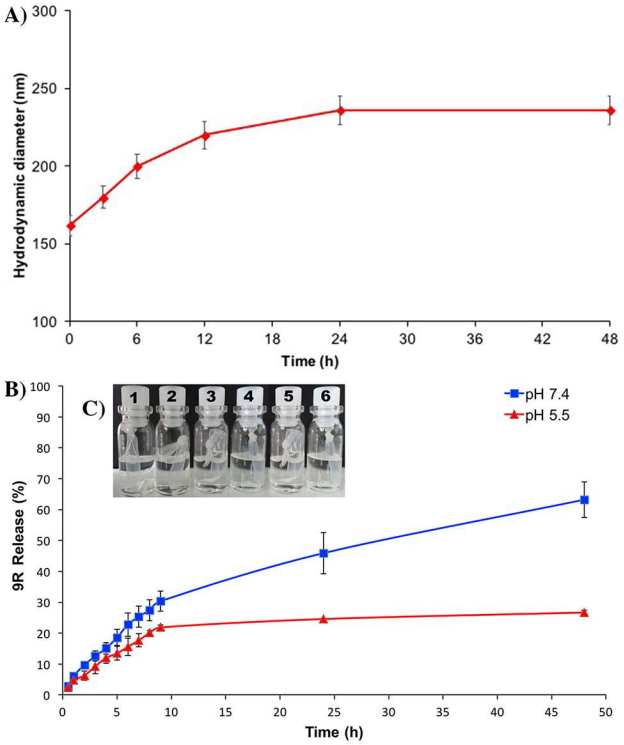

Figure 3. A) NPs stability studies were carried out in PBS at 37°C by monitoring particles diameter during time by DLS measurements. B) Cumulative release of 9R from 9R@ker nanoparticles in physiological conditions (pH = 7.4, blue line) and in acidic conditions (pH= 5.5, red line) at 37°C. C) 1mL of 9R@ker dispersion (7mg/mL) was placed into six dialysis bags (cut-off 12-14 kDa), and immersed in PBS at pH 7.4 (vials 1, 2 and 3) and at pH 5.5 (vials 4, 5 and 6) at 37°C.

As shown in Figure 3B, during the first 9 h, a burst release (up to 30%) occurred under both conditions; in the following time frame (48 h), a continuous slow release was observed at pH 7.4, whereas at pH 5.5 the release rate reached a plateau and the total 9R released was 26%, indicating that 9R release depends on the pH of the PBS solution. In order to explain this behavior, we measured the dimensions and zeta-potential of 9R@ker at different pH values (Table S1). Our results suggest that, under acidic conditions (pH = 5.5 and 4.5), a partial protonation of keratin sulfonic moieties on the NPs could take place, thus reducing the overall electrical repulsion among particles and favoring their aggregation and stability. This behavior could be beneficial for drug delivery purposes, allowing for a more controlled release of 9R and resulting in a prolonged therapeutic effect.

In order to establish the release kinetic and mechanism of 9R from keratin nanoparticles, different mathematical models were applied to experimental data. In particular, the kinetic of 9R release at different pH was described through empirical models, such as zero order linear equation, exponential first order equation and Higuchi square root of time equation. In addition, semi-empirical Peppas-Salhin and Korsemeyer-Peppas models were applied to investigate the drug release mechanism. R^2 values define the best fitting models (Table S2). As for the empirical models, the R^2 values indicate that at both pH values, i.e. 7.4 and 5.5, the drug is released according the Higuchi model, thus mainly controlled by diffusion.[45]

Nevertheless, the Korsemeyer-Peppas model revealed a different release mechanism. In particular, at pH 7.4 9R is released through a combination of Fickian diffusion and matrix swelling ($0.45<n<1$), while at pH 5.5 the release occurs exclusively through Fickian diffusion ($n<0.45$).[46] The Peppas-Salhin equation was then applied to determine the Fickian kinetic constants k_1 and the matrix swelling kinetic constant k_2. As shown in Table S2, at pH 7.4 the k_1 is significantly higher than the k_2, meaning that the Fickian diffusion prevails on the matrix swelling. On the other hand, the k_2 constant assumes a non-significant negative value, confirming the total Fickian diffusion of drug from the keratin nanoparticles.

The effect of 9R and 9R@ker on cell proliferation

The effect of 50 μM 9R and 9R@ker on human colon carcinoma cell line, i.e. HT29, Caco-2 and HCT116, as well as on normal embryonic intestinal cell line (I407) was evaluated at 24, 48, and 72 h after treatment. In HT29 cells, 9R and 9R@ker caused a significant decrease of cell proliferation over time, as compared to control groups, with average rates of growth inhibition of 26 ± 2, 45 ± 3, and 49 ± 2 %; 46 ± 2, 44 ± 5.5, and 32.0 ± 0.7%, respectively (Fig. 4A, B). In HCT116 the antiproliferative effect induced by both agents was higher, reducing the proliferation of 51 ± 2, 54 ± 2, and 66 ± 6%; 70 ±11, 57 ± 1, and 61.0 ± 1.4% respectively (Fig. 4A, B). In Caco-2 cells, 9R reduced the cell growth over time of 17.2 ± 0.2, 39 ± 3, and 33 ± 1 %; interestingly, treatment with 9R@ker induced a significant antiproliferative effect only after 48 and 72 h, namely of 43 ± 6 and 45 ± 5%, respectively

(Fig. 4A, B). The delay on 9R@ker with respect to free 9R might be due to the slower internalization of 9R@ker. As expected, our data confirmed that neither agents, 9R@ker and 9R alone, produced significant inhibition in I407 normal cell (Fig. 4A, B)[14]. Overall, these data account for a greater activity of 9R@ker, especially on HT29 cells 24 h after treatment (26% *vs* 49%). In order to explain this behavior, we performed all the experiments to follow only using HT29 cells.

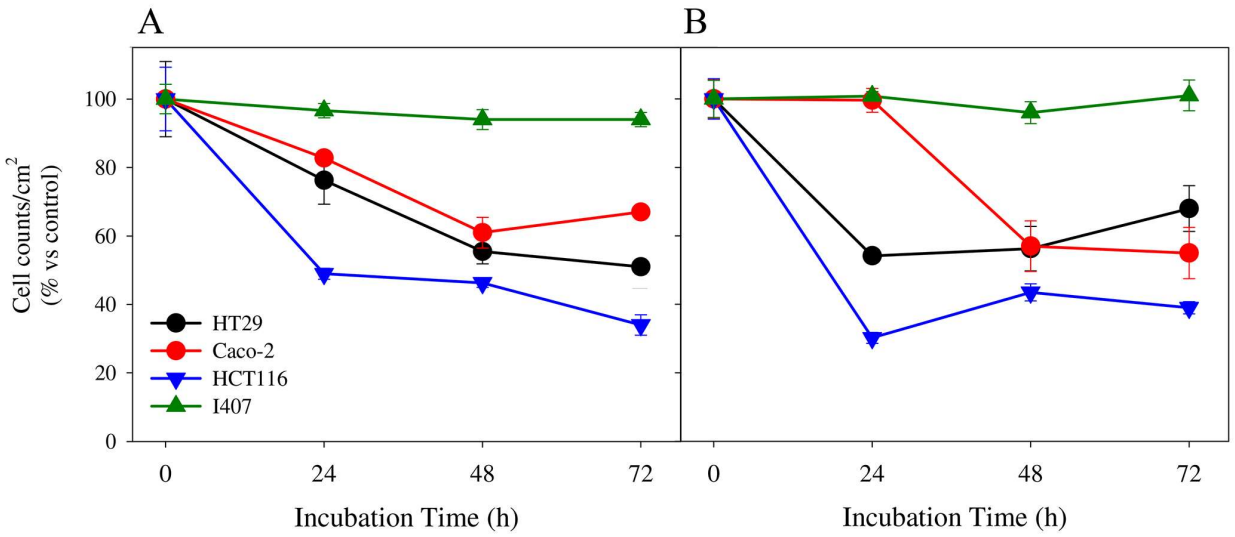

Figure 4. Antiproliferative effect of 9R (A) and 9R@ker (B) on HT29, Caco-2, HCT116 at 24, 48 and 72 h of treatment as compared with control. Results are expressed as means ± SD of three independent experiments.

***In vitro* cellular uptake.** In order to evaluate the efficiency of 9R cellular uptake once loaded onto keratin NPs, fluorescent keratin was synthesized by coupling pure keratin with fluorescein isothiocyanate (See supporting information). Fluorescent keratin (FITC:ker) was then used for the production of 9R loaded NPs (9R@FITC:ker) and of nude fluorescent nanoparticles (@FITC:ker). Cells internalization was evaluated through confocal microscopy, revealing that both particles are efficiently internalized already 15 min after treatment (Figure 5B and C); moreover, the presence of 9R does not affect the internalization degree (cfr. Figure 5B-C and 5D-E).

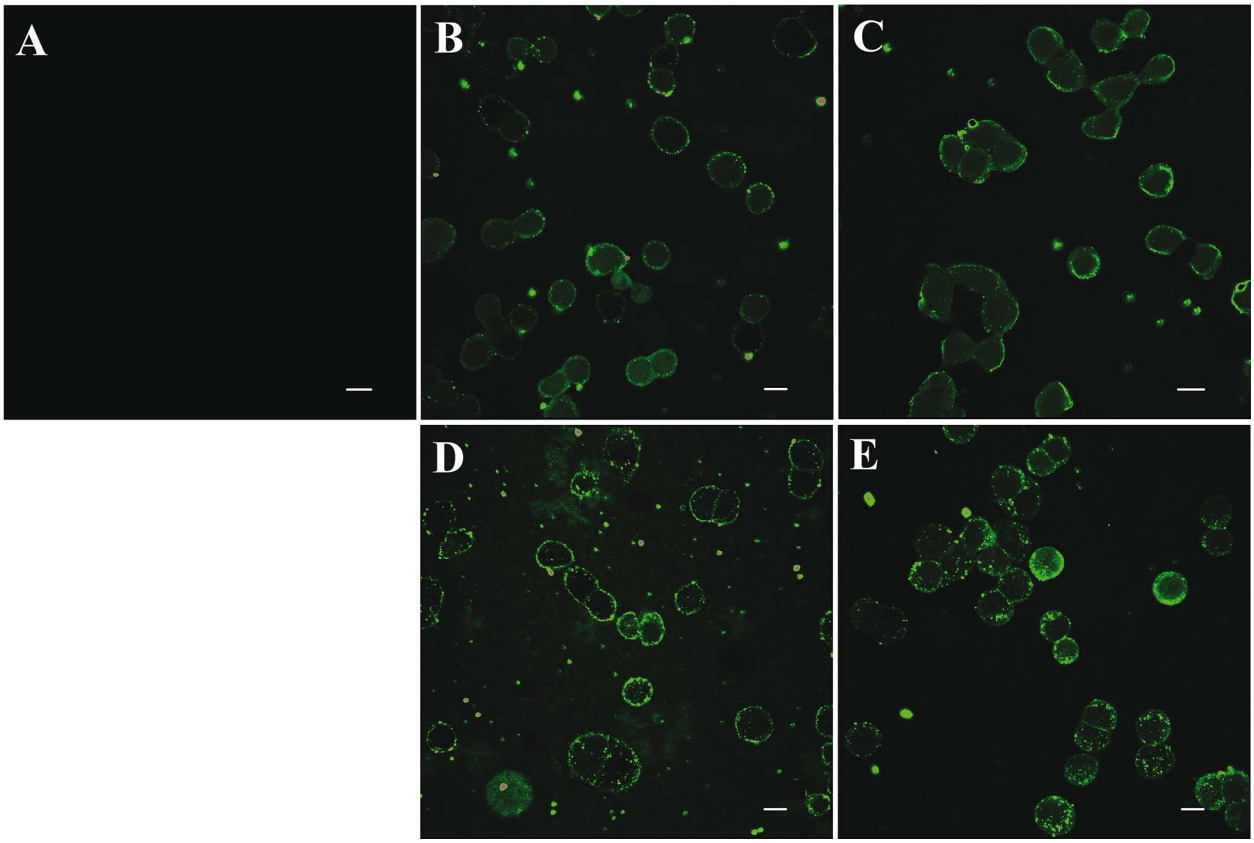

Figure 5. Fluorescence confocal microscopy of HT29 cells after incubation with NPs. The green fluorescence indicates the accumulation of 9R@FITC:ker for 15' (B) and 60' (D), and accumulation of @FITC:ker for 15' (C) and 60' (E); panel (A) reports the negative control (scale bar 10 μm).

Modulation of HT29 plasma membrane. To clarify the property changes of HT29 plasma membrane upon treatment with NPs, cells were stained with Nile Red (NR), a hydrophobic organic dye used for staining both polar and neutral lipids.[47] In fact, NR fluorescence may be examined either by excitation at 450-500 nm which produces a green fluorescence (530 nm), or at 549 nm which generates a red emission signal at 628 nm. Thus, non-polar lipids have been identified by green fluorescent structures, while polar lipids are visualized as red fluorescent structures;[48] this behavior allows to selectively investigate the effect of a drug on both polar and non-polar lipids composing the cell membrane.

HT29 cells stained with NR were treated with 9R@ker and 9R albumin nanoparticles (9R@HSAr) at a 9R equivalent concentration of 50 μM for 1h, followed by confocal microscopy analysis (Figure 6A, B). With the aim of investigating whether the effect of 9R@ker on the membrane organization

could be ascribed to the protein folding induced by the acid, (*12R*)-12-hydroxystearic acid (indicated hereafter as 12R) was selected to be loaded onto NPs (12R@ker). In fact, 12R exhibits similar chemical properties to 9R while it has no biological effect on HDAC1. Therefore, cells were incubated with 12R@ker (10 μM) for 1 hour before confocal microscopy analysis (Figure 6C). Our results show that 9R@HSAr does not affect HT29 membrane lipid organization, while 9R@ker significantly increases the exposure of nonpolar membrane lipids, thus indicating a specific effect induced by keratin as a carrier (Figure 6B, D). As an additional proof, the treatment with 12R@ker significantly increased the exposure of both lipid components, indicating that keratin plays a key role in inducing a change in the lipid bilayer organization (Figure 6A, C and D).

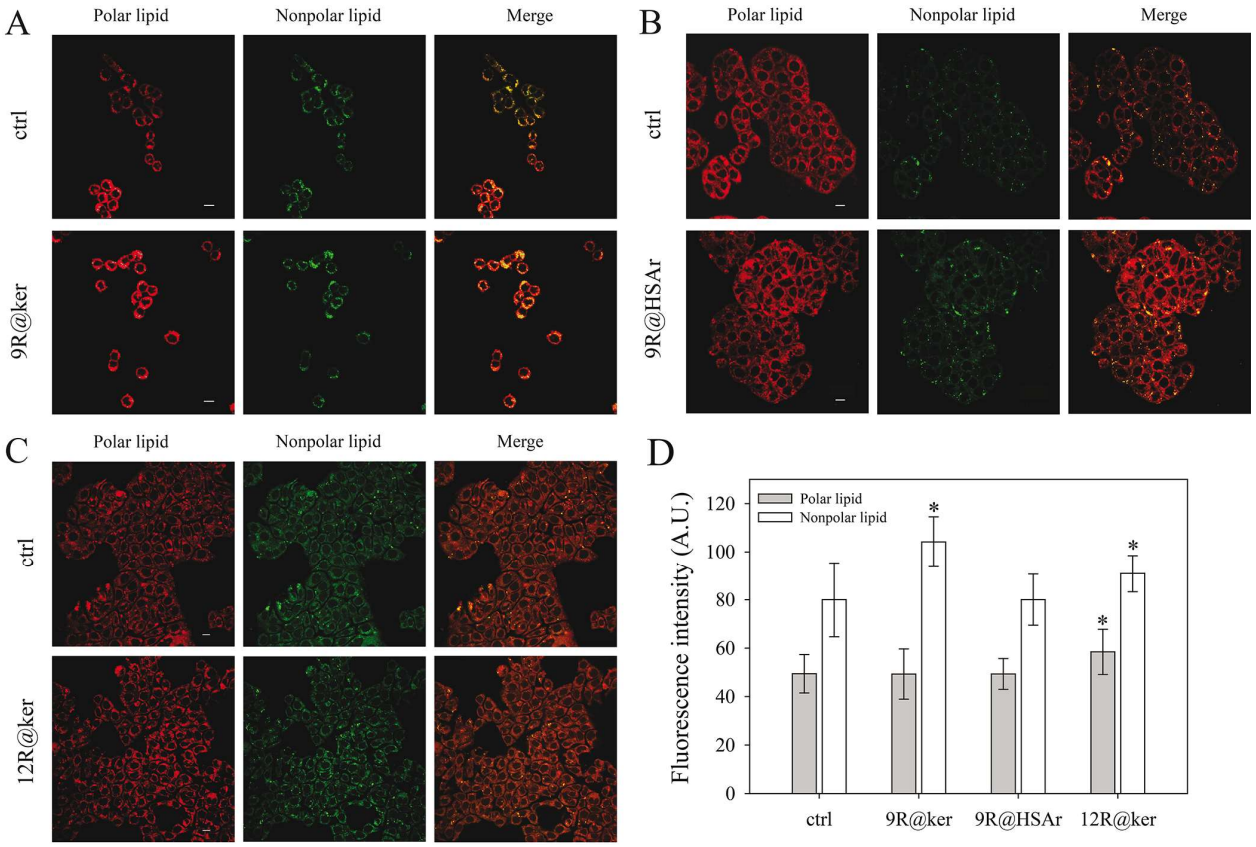

Figure 6. Modulation of HT29 plasma membrane properties by NPs. Fluorescence intensities of HT29 cells incubated with 9R@ker (A), 9R@HSAr (B) and 12R@ker (C) for 1 hour, then stained with NR. Representative images are shown. D) Image densitometry was measured using ImageJ (* $p<0.05$ respect to control).

The possible modifications induced by 9R@ker and 12R@ker on the physico-chemical state of human HT29 cell membranes were investigated through steady-state fluorescence anisotropy, using TMA-DPH (1-(4-Trimethylammoniumphenyl)-6-Phenyl-1,3,5-Hexatriene p-Toluenesulfonate) as a fluorescent probe. In the absence of NPs (control) as well as in the presence of 12R@ker, an anisotropy value of 0.27 ± 0.01 was measured (Figure 7A), while in the presence of 9R@ker a significant decrease in TMA-DPH anisotropy (0.25 ± 0.01) was observed. In addition, the production of intracellular reactive oxygen species (ROS) was detected upon treatment with 9R@ker. Cellular oxidative stress was measured by means of the cell-permeant probe H2DCF-DA.[49] Even though DCF does not discriminate between the different reactive oxygen/nitrogen species, it remains the reference indicator for an easy detection of cellular oxidative stress.[49] HT29 cells were exposed to *tert*-butylhydroperoxide (TBH) as a positive control, while untreated and unstained cells represent the negative control. As shown in Figure 7B, only 9R@ker significantly increased HT29 ROS content.

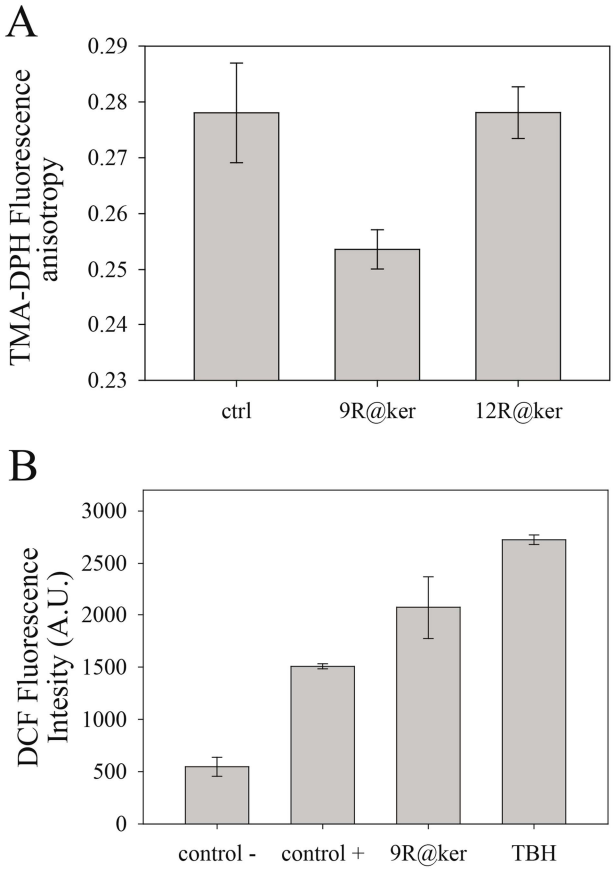

Figure 7. TMA-DPH anisotropy and intracellular ROS production in control and NPs treated HT29 cells. A) TMA-DPH anisotropy in HT29 cells control, treated with 9R@ker or 12R@ker. B)

Intracellular ROS production in control and 9R@ker treated HT29 cells. ROS production was evaluated by H2DCF-DA fluorescent assay. Ctrl - : untreated and unstained cells; TBH: tert-butylhydroperoxide treated cells; control HT29 cells (ctrl +) or treated with 9R@ker (* $p<0.05$ respect to control).

Biological effect. Viable HT29 cells were counted 24 h after treatment with 50 μM 9R, or 9R@ker, or 9R@HSAr, or @ker, or keratin alone or 10 μM 12R@ker, or 12R-in order to evaluate the effect on cell proliferation. As expected, @ker and keratin induced a slight increase in the number of cells (Figure 8A) characterized by a faster exit from G0/G1 phase of the cell cycle (Figure 8B). Indeed, several findings have revealed that keratin plays fundamental roles in epithelial cells, such as the regulation of metabolic processes and pathways responsible of growth, proliferation and migration.[50] On the other hand, treatment with 9R, 9R@ker, and 9R@HSAr led to a reduction in cells number with respect to control (Figure 8A). The cell-cycle distribution of 9R, 9R@ker, 9R@HSAr, 12R@ker, 12R, @ker and keratin treated cells was analyzed by flow cytometry. Cells were exposed to compounds for 24 hours prior to processing and analysis. As shown in Figure 8B, treatment with 9R or 9R@HSAr resulted in an increase in the number of cells in the G0/G1 phase, while treatment with 9R@ker resulted in a significant increase of S phase cells. Given that this latter effect is not ascribable to 9R mechanism of action[6] and is not observed for 9R@HSAr, we might suppose that the specific effect induced by 9R@ker on cells proliferation is caused by a different mechanism of interaction with the plasma membrane, which results in an increase of ROS production that in turn triggers a different signal transduction.

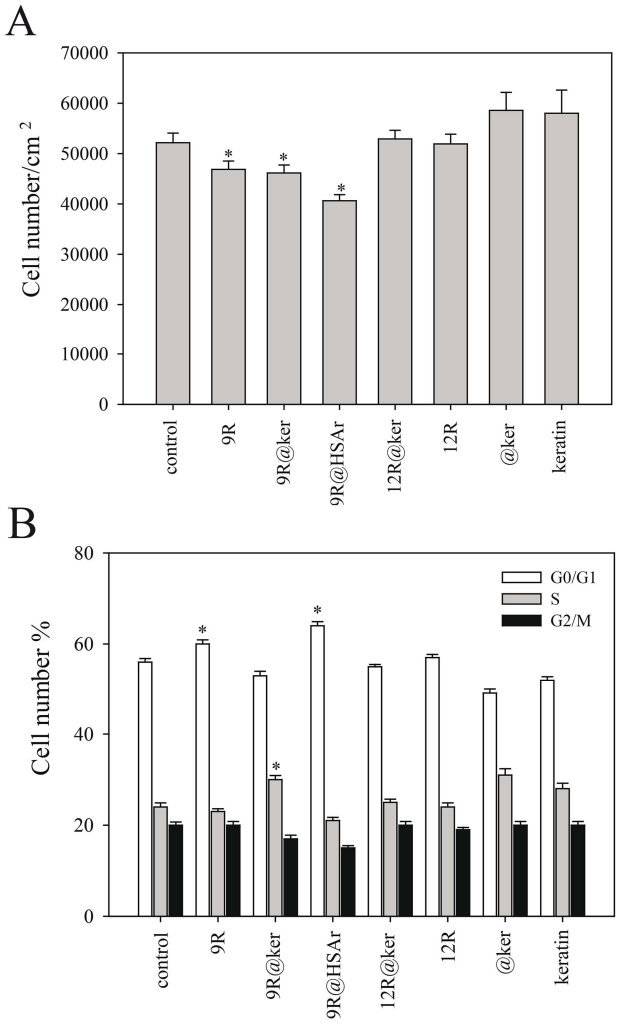

Figure 8. Effects on cell proliferation and cell cycle analysis. A) Cell viability of HT29 cells after treatment with 50 μM 9R, 9R@ker, 9R@HSAr, @ker and keratin and 10 μM 12R@ker, 12R as compared with untreated cells. B) HT29 nuclei were isolated, stained with propidium iodide (PI) and analyzed by flow cytometry. The significant values represent mean ± SD of three independent experiments.

In order to identify acetylated histones, we analyzed the nuclear cell lysates by western blot analysis using a pan-anti-acetyl lysine monoclonal antibody. In details, the antibody could reveal the acetylated proteins accumulation induced in HT29 cells treated with 9R, or 9R@ker, or @ker, or keratin (Figure 9A), and 9R, or 9R@HSAr, or 12R@ker (Figure 9C). Differences in bands density might detect modifications in protein acetylation levels. Histone acetylation signals were quantified by densitometry and normalized on histone H1 (Figures 9B and D).

An altered effect on histones acetylation was observed in HT29 cells upon treatment with 9R, or 9R@HSAr, or 9R@ker for 6 h. In particular, 9R and 9R@HSAr induced H4 hyperacetylation (Figures 9A and B, lane 2 and Figures 9C and D, lanes 1 and 4), while 9R@ker induced H2/H3 hyperacetylation (Figures 9A and B, lane 3).

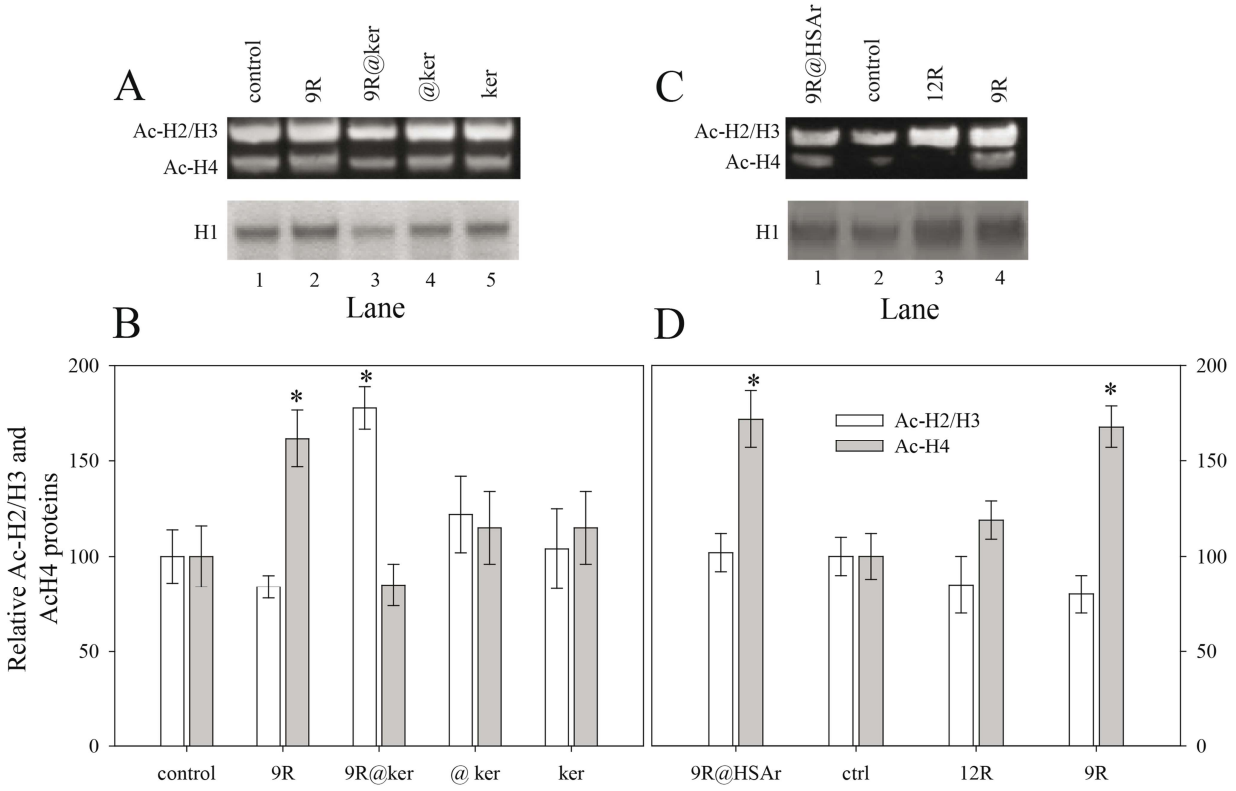

Figure 9. NPs triggers histone acetylation and DNA expression in HT29 cells. A) Cells were treated with 9R, 9R@ker, @ker and keratin. B) Protein contents of acetylated histones H2/H3 (Ac-H2/H3) and H4 (Ac-H4) from image densitometry measured using ImageJ. C) Cells were treated with 9R@HSAr, 12R and 9R@ker. D) Protein contents of acetylated histones H2/H3 (Ac-H2/H3) and H4 (Ac-H4) from image densitometry measured using ImageJ. Mean ± SEM, n = 3, *: $P < 0.05$.

p21^{WAF1} and *Bax* transcription levels were analyzed by RT-PCR, indicating that *p21*^{WAF1} gene expression was upregulated both by 9R and ~~or~~ 9R@ker by a factor of 3.24 and 2.79 (Figure 10A), while the protein level increased of 16% and 37%, respectively (Figures 10B and C). On the other hand, a significant *Bax* gene transcription upregulation was observed only in cells treated with 9R@ker by a factor of 2.42 ($p \leq 0.001$), resulting on a 35% increase of Bax protein as respect to

control. The different histones epigenetic modifications lead to different transcriptional effects: H4 hyperacetylation induces an increased $p21^{WAF1}$ gene expression with G0/G1 phase cell cycle arrest (Figure 7B), while H2/H3 hyperacetylation induces an increased gene expression of both $p21^{WAF1}$ and *Bax* with consequent accumulation of cells in S phase and cell death (Figures 8).

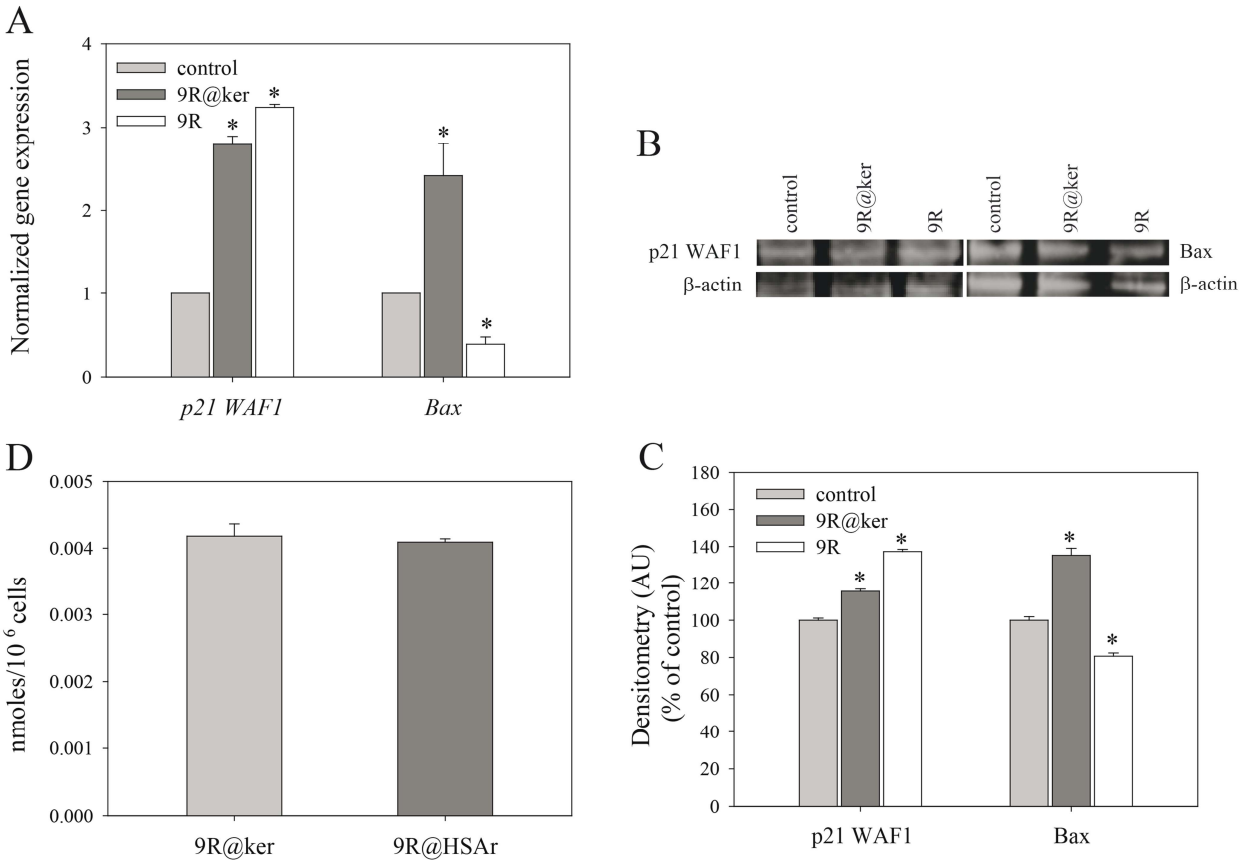

Figure 10. A) p21WAF1 and Bax normalized gene expression analyzed by qRT-PCR. Data are expressed as mean values of the relative variation (fold change) of treated *vs* control samples. Data are representative of three independent experiments. *$p \leq 0.01$ vs control. B) Western blot of p21 and Bax level in HT29 cells, evaluated 24 h after treatment with 9R@ker or 9R. C) Proteins western blot quantification, normalized to β-actin band. Bars represent mean values based on three independent experiments, error bar represent SD. D) 9R intracellular concentration determined by ESI-mass spectrometry.

In our opinion, these effects cannot be ascribed to a different 9R intracellular concentration; in fact, as shown in Figure 10D, the free acid concentration is essentially the same for cells treated with

9R@ker ($4.18 \times 10^{-3} \pm 1.85 \times 10^{-4}$ cells) or 9R@HSAr ($4.09 \times 10^{-3} \pm 5 \times 10^{-5}$ cells) and corresponds to that previously determined for free 9R.[6]

Interestingly, treatment of HT29 cells with free 9R leads to downregulation of *Bax* gene expression by a factor of 0.4 ($P \leq 0.001$) inducing a 20% decrease of protein content as compared to control. One possible explanation of this behavior might be related to a gene reprogramming towards a benign differentiation,[35] however, a more detailed study is ongoing in order to clarify this behavior.

CONCLUSION

Altered expression of individual histone deacetylases HDACs is often found in tumor samples. It has been found that the (*R*) enantiomer of 9-hydroxystearic acid (9R) is able to effectively inhibit HDAC1 at micromolar concentration causing growth inhibition of colon cancer cells. Despite its promising activity, 9R lacks suitable water solubility and pharmacokinetic profile. In this work we present the production of highly stable and reproducible keratin nanoparticles loaded with 9R through a drug-induced aggregation method (9R@ker). Our data demonstrate that once loaded on keratin, 9R exerts a different effect on HT29 cells especially in terms of plasma membrane interaction and effect on cell cycle. In particular, 9R@ker increase membrane fluidity and the exposure of nonpolar membrane lipids. Moreover, results herein presented account for higher intracellular ROS formation induced only by 9R@ker that seems to be correlated to a higher percentage of cancer cells in S phase instead of G0/G1 phase, as normally induced by free 9R. Overall these preliminary results constitute an encouraging rationale for further *in vitro* and *in vivo* evaluation of 9R@ker for the treatment of colon cancer.

ASSOCIATED CONTENT

Supporting Information. The Supporting Information is available free of charge on the ACS Publications website at DOI: detailed description of @ker, @ FITC:ker, 9R@ FITC:ker, *d*9@ker, 12R@ker, @HSAr and 9R@HSAr, *d*9@HSAr synthesis and characterization data, hydrodynamic

diameter, polydispersity index and drug loading, empirical and semi-empirical models for release mechanism, LC-MS analysis and chromatograms (PDF).

AUTHOR INFORMATION

Corresponding Author

*Dr. Greta Varchi – Italian National Research Council – Institute of Organic Synthesis and Photoreactivity Via P. Gobetti, 101, 40129 Bologna (ITALY). Phone +390516398283; Fax +390516398349 Email greta.varchi@isof.cnr.it

*Dr. Natalia Calonghi – Department of Pharmacy and Biotechnology, Via Irnerio 48, 40126 Bologna (ITALY). Phone +390512091231 Email natalia.calonghi@unibo.it

Author Contributions

The manuscript was written through contributions of all authors. All authors have given approval to the final version of the manuscript.

Funding Sources

This work was supported by the Investigator Grant of the Italian Association for Cancer Research (AIRC) 16740 to G.V. and ALMA MATER STUDIORUM – Università di Bologna (ex-RFO funds) to C.B. and N.C.

ACKNOWLEDGMENT

Authors thank Dr. G. Micheletti of University of Bologna for the assistance in 9R synthesis.

ABBREVIATIONS

Keratin NPs (@ker), fluorescein isothiocyanate keratin NPs (@FITC:ker), 9R fluorescein isothiocyanate loaded keratin NPs (9R@FITC:ker), deuterated 9-HSA keratin NPs (*d*9@ker),

(*12R*)-12-hydroxy stearic acid keratin NPs (12R@ker), albumin NPs (@HSAr) and deuterated 9-HSA albumin NPs (*d*9@HSAr) as reference system.

REFERENCES

(1) Fraga, M. F.; Ballestar, E.; Villar-Garea, A.; Boix-Chornet, M.; Espada, J.; Schotta, G.; Bonaldi, T.; Haydon, C.; Ropero, S.; Petrie, K.; et al. Loss of Acetylation at Lys16 and Trimethylation at Lys20 of Histone H4 Is a Common Hallmark of Human Cancer. *Nat. Genet.* **2005**, *37* (4), 391–400.

(2) Yasui, W.; Oue, N.; Ono, S.; Mitani, Y.; Ito, R.; Nakayama, H. Histone Acetylation and Gastrointestinal Carcinogenesis. *Ann. N. Y. Acad. Sci.* **2003**, *983* (1), 220–231.

(3) Ceccacci, E.; Minucci, S. Inhibition of Histone Deacetylases in Cancer Therapy: Lessons from Leukaemia. *Br. J. Cancer* **2016**, *114* (6), 605–611.

(4) Liu, T.; Kapustin, G.; Etzkorn, F. A. Design and Synthesis of a Potent Histone Deacetylase Inhibitor. *J. Med. Chem.* **2007**, *50* (9), 2003–2006.

(5) Ropero, S.; Esteller, M. The Role of Histone Deacetylases (HDACs) in Human Cancer. *Mol. Oncol.* **2007**, *1* (1), 19–25.

(6) Calonghi, N.; Cappadone, C.; Pagnotta, E.; Boga, C.; Bertucci, C.; Fiori, J.; Tasco, G.; Casadio, R.; Masotti, L. Histone Deacetylase 1: A Target of 9-Hydroxystearic Acid in the Inhibition of Cell Growth in Human Colon Cancer. *J. Lipid Res.* **2005**, *46* (8), 1596–1603.

(7) Juan, L.-J.; Shia, W.-J.; Chen, M.-H.; Yang, W.-M.; Seto, E.; Lin, Y.-S.; Wu, C.-W. Histone Deacetylases Specifically Down-Regulate P53-Dependent Gene Activation. *J. Biol. Chem.* **2000**, *275* (27), 20436–20443.

(8) Xu, W. S.; Parmigiani, R. B.; Marks, P. A. Histone Deacetylase Inhibitors: Molecular Mechanisms of Action. *Oncogene* **2007**, *26* (37), 5541–5552.

(9) Calonghi, N.; Pagnotta, E.; Parolin, C.; Tognoli, C.; Boga, C.; Masotti, L. 9-Hydroxystearic Acid Interferes with EGF Signalling in a Human Colon Adenocarcinoma. *Biochem. Biophys. Res. Commun.* **2006**, *342* (2), 585–588.

(10) Masotti, L.; Casali, E.; Gesmondo, N.; Sartor, G.; Galeotti, T.; Borrello, S.; Piretti, M. V.; Pagliuca, G. Lipid Peroxidation in Cancer Cells: Chemical and Physical Studies. *Ann. N. Y. Acad. Sci.* **1988**, *551* (1), 47–57.

(11) Gui, C.-Y.; Ngo, L.; Xu, W. S.; Richon, V. M.; Marks, P. A. Histone Deacetylase (HDAC) Inhibitor Activation of P21WAF1 Involves Changes in Promoter-Associated Proteins, Including HDAC1. *Proc. Natl. Acad. Sci.* **2004**, *101* (5), 1241–1246.

(12) Zhang, Z.; Yamashita, H.; Toyama, T.; Sugiura, H.; Ando, Y.; Mita, K.; Hamaguchi, M.; Hara, Y.; Kobayashi, S.; Iwase, H. Quantitation of HDAC1 MRNA Expression in Invasive Carcinoma of the Breast*. *Breast Cancer Res. Treat.* **2005**, *94* (1), 11–16.

(13) Calonghi, N.; Pagnotta, E.; Parolin, C.; Molinari, C.; Boga, C.; Dal Piaz, F.; Brusa, G. L.; Santucci, M. A.; Masotti, L. Modulation of Apoptotic Signalling by 9-Hydroxystearic Acid in Osteosarcoma Cells. *Biochim. Biophys. Acta* **2007**, *1771* (2), 139–146.

(14) Gesmundo, N.; Casali, E.; Farruggia, G.; Spisni, A.; Masotti, L. In Vitro Effects of Hydroxystearic Acid on the Proliferation of HT29 and I407 Cells. *Biochem. Mol. Biol. Int.* **1994**, *33* (4), 705–712.

(15) Casali, E.; Gesmundo, N.; Farruggia, G.; Spisni, A.; Masotti, L. Hydroxystearic Acid Effects on CDC2/Histone H1 Kinase Activity in C108 Carcinoma Cells. *Biochem. Biophys. Res. Commun.* **1994**, *203* (3), 1385–1391.

(16) Calonghi, N.; Cappadone, C.; Pagnotta, E.; Farruggia, G.; Buontempo, F.; Boga, C.; Brusa, G. .; Santucci, M. .; Masotti, L. 9-Hydroxystearic Acid Upregulates P21 WAF1 in HT29 Cancer Cells. *Biochem. Biophys. Res. Commun.* **2004**, *314* (1), 138–142.

(17) Parolin, C.; Calonghi, N.; Presta, E.; Boga, C.; Caruana, P.; Naldi, M.; Andrisano, V.; Masotti, L.; Sartor, G. Mechanism and Stereoselectivity of HDAC I Inhibition by (R)-9-Hydroxystearic Acid in Colon Cancer. *Biochim. Biophys. Acta - Mol. Cell Biol. Lipids* **2012**, *1821* (10), 1334–1340.

(18) Boanini, E.; Torricelli, P.; Boga, C.; Micheletti, G.; Cassani, M. C.; Fini, M.; Bigi, A. (9R)-9-Hydroxystearate-Functionalized Hydroxyapatite as Antiproliferative and Cytotoxic Agent toward Osteosarcoma Cells. *Langmuir* **2016**, *32* (1), 188–194.

(19) Iyer, A. K.; Khaled, G.; Fang, J.; Maeda, H. Exploiting the Enhanced Permeability and Retention Effect for Tumor Targeting. *Drug Discov. Today* **2006**, *11* (17–18), 812–818.

(20) Boanini, E.; Cassani, M.; Rubini, K.; Boga, C.; Bigi, A. (9R)-9-Hydroxystearate-Functionalized Anticancer Ceramics Promote Loading of Silver Nanoparticles. *Nanomaterials* **2018**, *8* (6), 390.

(21) Jahanshahi, M.; Babaei, Z. Protein Nanoparticle: A Unique System as Drug Delivery Vehicles. *African J. Biotechnol.* **2008**, *7* (25), 4926–4934.

(22) Lohcharoenkal, W.; Wang, L.; Chen, Y. C.; Rojanasakul, Y. Protein Nanoparticles as Drug Delivery Carriers for Cancer Therapy. *Biomed Res. Int.* **2014**, *2014*, 1–12.

(23) Aluigi, A.; Sotgiu, G.; Ferroni, C.; Duchi, S.; Lucarelli, E.; Martini, C.; Posati, T.; Guerrini, A.; Ballestri, M.; Corticelli, F.; et al. Chlorin E6 Keratin Nanoparticles for Photodynamic Anticancer Therapy. *RSC Adv.* **2016**, *6* (40), 33910–33918.

(24) Zhi, X.; Wang, Y.; Li, P.; Yuan, J.; Shen, J. Preparation of Keratin/Chlorhexidine Complex Nanoparticles for Long-Term and Dual Stimuli-Responsive Release. *RSC Adv.* **2015**, *5* (100), 82334–82341.

(25) Li, Y.; Zhi, X.; Lin, J.; You, X.; Yuan, J. Preparation and Characterization of DOX Loaded Keratin Nanoparticles for PH/GSH Dual Responsive Release. *Mater. Sci. Eng. C* **2017**, *73*, 189–197.

(26) Aluigi, A.; Ballestri, M.; Guerrini, A.; Sotgiu, G.; Ferroni, C.; Corticelli, F.; Gariboldi, M. B.; Monti, E.; Varchi, G. Organic Solvent-Free Preparation of Keratin Nanoparticles as Doxorubicin Carriers for Antitumour Activity. *Mater. Sci. Eng. C* **2018**, *90*, 476–484.

(27) Foglietta, F.; Spagnoli, G. C.; Muraro, M. G.; Ballestri, M.; Guerrini, A.; Ferroni, C.; Aluigi, A.; Sotgiu, G.; Varchi, G. Anticancer Activity of Paclitaxel-Loaded Keratin Nanoparticles in Two-Dimensional and Perfused Three-Dimensional Breast Cancer Models. *Int. J. Nanomedicine* **2018**, *13*, 1–21.

(28) Ferroni, C.; Sotgiu, G.; Sagnella, A.; Varchi, G.; Guerrini, A.; Giuri, D.; Polo, E.; Orlandi, V. T.; Marras, E.; Gariboldi, M.; et al. Wool Keratin 3D Scaffolds with Light-Triggered Antimicrobial Activity. *Biomacromolecules* **2016**, *17* (9), 2882–2890.

(29) Gradishar, W. J.; Tjulandin, S.; Davidson, N.; Shaw, H.; Desai, N.; Bhar, P.; Hawkins, M.; O'Shaughnessy, J. Phase III Trial of Nanoparticle Albumin-Bound Paclitaxel Compared With Polyethylated Castor Oil–Based Paclitaxel in Women With Breast Cancer. *J. Clin. Oncol.* **2005**, *23* (31), 7794–7803.

(30) Yang, Q.; Qiu, H.; Guo, W.; Wang, D.; Zhou, X.; Xue, D.; Zhang, J.; Wu, S.; Wang, Y. Quantitative 1H-NMR Method for the Determination of Tadalafil in Bulk Drugs and Its Tablets. *Molecules* **2015**, *20* (7), 12114–12124.

(31) Ebert, C.; Felluga, F.; Forzato, C.; Foscato, M.; Gardossi, L.; Nitti, P.; Pitacco, G.; Boga, C.; Caruana, P.; Micheletti, G.; et al. Enzymatic Kinetic Resolution of Hydroxystearic Acids: A Combined Experimental and Molecular Modelling Investigation. *J. Mol. Catal. B Enzym.* **2012**, *83*, 38–45.

(32) Aridoss, G.; Laali, K. K. Ethylammonium Nitrate (EAN)/Tf 2 O and EAN/TFAA: Ionic Liquid Based Systems for Aromatic Nitration. *J. Org. Chem.* **2011**, *76* (19), 8088–8094.

(33) Posati, T.; Giuri, D.; Nocchetti, M.; Sagnella, A.; Gariboldi, M.; Ferroni, C.; Sotgiu, G.; Varchi, G.; Zamboni, R.; Aluigi, A. Keratin-Hydrotalcites Hybrid Films for Drug Delivery Applications. *Eur. Polym. J.* **2018**, *105*, 177–185

(34) Abruzzo, A.; Zuccheri, G.; Belluti, F.; Provenzano, S.; Verardi, L.; Bigucci, F.; Cerchiara, T.; Luppi, B.; Calonghi, N. Chitosan Nanoparticles for Lipophilic Anticancer Drug Delivery: Development, Characterization and in Vitro Studies on HT29 Cancer Cells. *Colloids Surf. B* **2016**, *145*, 362–372.

(35) Pagnotta, E.; Calonghi, N.; Boga, C.; Masotti, L. N-Methylformamide and 9-Hydroxystearic Acid: Two Anti-Proliferative and Differentiating Agents with Different Modes of Action in Colon Cancer Cells. *Anticancer. Drugs* **2006**, *17* (5), 521–526.

(36) Amellem, O.; Stokke, T.; Sandvik, J. A.; Pettersen, E. O. The Retinoblastoma Gene Product Is Reversibly Dephosphorylated and Bound in the Nucleus in S and G2 Phases during Hypoxic Stress. *Exp. Cell Res.* **1996**, *227* (1), 106–115.

(37) Hoffmann; Cinatl; Kabicková; Kreuter; Stieneker. Preparation, Characterization and Cytotoxicity of Methylmethacrylate Copolymer Nanoparticles with a Permanent Positive Surface Charge. *Int. J. Pharm.* **1997**, *157* (2), 189–198.

(38) Duchi, S.; Sotgiu, G.; Lucarelli, E.; Ballestri, M.; Dozza, B.; Santi, S.; Guerrini, A.; Dambruoso, P.; Giannini, S.; Donati, D.; Ferroni, C.; Varchi, G. Mesenchymal Stem Cells as Delivery Vehicle of Porphyrin Loaded Nanoparticles: Effective Photoinduced in Vitro Killing of Osteosarcoma. *J. Control. Release* **2013**, *168*, 225–237.

(39) Wang, K.; Li, R.; Ma, J. H.; Jian, Y. K.; Che, J. N. Extracting Keratin from Wool by Using L-Cysteine. *Green Chem.* **2016**, *18* (2), 476–481.

(40) Maloisel, L.; Fabre, F.; Gangloff, S. DNA Polymerase Delta Is Preferentially Recruited during Homologous Recombination to Promote Heteroduplex DNA Extension. *Mol. Cell. Biol.* **2008**, *28* (4), 1373–1382.

(41) Holzwarth, G.; Doty, P. The Ultraviolet Circular Dichroism of Polypeptdes. *J. Am. Chem. Soc.* **1965**, *87*, 218–228.

(42) Venyaminov SYu; Baikalov, I. A.; Shen, Z. M.; Wu, C. S.; Yang, J. T. Circular Dichroic Analysis of Denatured Proteins: Inclusion of Denatured Proteins in the Reference Set. *Anal. Biochem.* **1993**, *214* (1), 17–24.

(43) Zhang, X.; Meng, L.; Lu, Q.; Fei, Z.; Dyson, P. J. Targeted Delivery and Controlled Release of Doxorubicin to Cancer Cells Using Modified Single Wall Carbon Nanotubes. *Biomaterials* **2009**, *30* (30), 6041–6047.

(44) Fareghi-Alamdari, R.; Zandi, F.; Keshavarz, M. H. Copper–Cobalt Synergy in Cu 1−x Co x Fe 2 O 4 Spinel Ferrite as a Highly Efficient and Regioselective Nanocatalyst for the Synthesis of 2,4-Dinitrotoluene. *RSC Adv.* **2015**, *5* (88), 71911–71921.

(45) Ghosal, K.; Chandra, A.; Rajabalaya, R.; Chakraborty, S.; Nanda, A. Mathematical Modeling of Drug Release Profiles for Modified Hydrophobic HPMC Based Gels. *Pharmazie* **2012**, *67* (2), 147–155.

(46) Li, N.-N.; Fu, C.-P.; Zhang, L.-M. Using Casein and Oxidized Hyaluronic Acid to Form Biocompatible Composite Hydrogels for Controlled Drug Release. *Mater. Sci. Eng. C. Mater. Biol. Appl.* **2014**, *36*, 287–293.

(47) Greenspan, P.; Mayer, E. P.; Fowler, S. D. Nile Red: A Selective Fluorescent Stain for Intracellular Lipid Droplets. *J. Cell Biol.* **1985**, *100* (3), 965–973.

(48) Brown, W. J.; Sullivan, T. R.; Greenspan, P. Nile Red Staining of Lysosomal Phospholipid Inclusions. *Histochemistry* **1992**, *97* (4), 349–354.

(49) Kalyanaraman, B.; Darley-Usmar, V.; Davies, K. J. A.; Dennery, P. A.; Forman, H. J.; Grisham, M. B.; Mann, G. E.; Moore, K.; Roberts, L. J.; Ischiropoulos, H. Measuring Reactive Oxygen and Nitrogen Species with Fluorescent Probes: Challenges and Limitations. *Free Radic. Biol. Med.* **2012**, *52* (1), 1–6.

(50) Pan, X.; Hobbs, R. P.; Coulombe, P. A. The Expanding Significance of Keratin Intermediate Filaments in Normal and Diseased Epithelia. *Curr. Opin. Cell Biol.* **2013**, *25* (1), 47–56.

Table of Contents